$Synthesis \ and \ electrocatalytic \ applications \ of \ flower-like \ motifs$ and associated composites of nitrogen-enriched tungsten nitride (W2N3)

Sha Tan, ¹ Brian M. Tackett, ² Qun He, ² Ji Hoon Lee, ² Jingguang G. Chen^{2,3,*}, and Stanislaus S. Wong^{1,*}

Email: jgchen@columbia.edu; stanislaus.wong@stonybrook.edu

¹Department of Chemistry, State University of New York at Stony Brook, Stony Brook, NY 11794-3400

²Department of Chemical Engineering, Columbia University, New York, NY 10027

³Chemistry Department, Building 555, Brookhaven National Laboratory,

Upton, NY 11973

*To whom correspondence should be addressed

Keywords: tungsten nitride, synthesis, composite, morphology control, electrocatalysis

Abstract. We have sought to improve the electrocatalytic performance of tungsten nitride through synthetic control over chemical composition and morphology. In particular, we have generated a thermodynamically unstable but catalytically promising nitrogen-rich phase of tungsten via a hydrothermal generation of a tungsten oxide intermediate and subsequent annealing in ammonia. The net product consisted of three-dimensional (3D) micron-scale flowerlike motifs of W₂N₃; this architecture not only evinced high structural stability but also incorporated the favorable properties of constituent two-dimensional nanosheets. From a performance perspective, as-prepared 3D W₂N₃ demonstrated promising hydrogen evolution reaction (HER) activities, especially in an acidic environment with a measured overpotential value of -101 mV at a current density of 10 mA/cm². To further enhance the electrocatalytic activity, small amounts of precious metal nanoparticles (such as Pt and Au), consisting of variable sizes, were uniformly deposited onto the underlying 3D W₂N₃ motifs using a facile direct deposition method; these composites were applied towards the CO₂ reduction reaction (CO₂RR). A highlight of this series of experiments was that Au/W₂N₃ composites were found to be a much more active HER (as opposed to either a CO₂RR or a methanol oxidation reaction (MOR)) catalyst.

1. Introduction

From the viewpoint of applications, transition metal nitrides (TMNs) are particularly intriguing, owing to their unique physical and chemical properties, especially in the context of different types of catalysis reactions,[1] including but not limited to hydrodesulfurization (HDS), the hydrogen evolution reaction (HER), the oxygen reduction reaction (ORR), and the methanol oxidation reaction (MOR).[2-4] One rationale is that the incorporation of nitrogen (or carbon) within the underlying transition metal framework expands the lattice, thereby enabling a contraction of the transition metal *d*-band. This favorable scenario gives rise to a greater electronic density of states (DOS) near the Fermi level as compared with the parent metal alone, with the practical consequence that TMNs possess an overall desirable catalytic activity similar in scope to that of less abundant and more expensive precious metals.[5]

As a subclass of TMNs, tungsten nitride (WN_x) can be generated with different phases, incorporating diverse chemical compositions (i.e., 'x' = 0.5 - 2.0), depending on the synthetic protocols involved. It has been reported that the metal-to-nitrogen ratio within TMNs significantly impacts upon their properties; specifically, the high nitrogen content as manifested in an abundance of metal-nitrogen bonds is likely responsible for the improved catalytic activity of nitrogen-rich TMN.[6] However, the conventional synthesis of nitrogen-rich WN_x tends to involve rather harsh conditions, i.e. high temperature and high pressure conditions; this is necessary, because integrating nitrogen atoms within an underlying W lattice is thermodynamically unfavorable under ambient conditions.[7] These serious issues with synthesis therefore render the equally important issue of desirable morphology control as an even more laborious and challenging task, especially at high temperatures and pressures.

Not surprisingly, W₂N₃, the most nitrogen-rich phase within the WN_x family, was only recently synthesized, but under relatively challenging high pressure and temperature (P-T) synthesis (5 GPa and 1223 K) conditions; the isolated morphology consisted of irregular plates.[7] Since then, a similar high P-T metathesis protocol was recently used to generate the corresponding W_{2,25}N₃. Moreover, a different ambient pressure, template-based process, incorporating a high-temperature annealing step, yielded 2D W₂N₃ flakes.[6, 8] Given this prior literature, there are obvious limitations associated with generating TMNs in general and tungsten nitrides in particular, under reasonably mild synthesis conditions with simultaneous control over both desired chemical composition and morphology. Specifically, there is an apparent scarcity of reliable synthetic processes necessary for fabricating nitrogen-rich W₂N₃.

To address these issues, herein, we are reporting on the nitridation of transition metal oxides (TMO) as a plausible means of simultaneously and reliably tuning both morphology and chemical composition. An added advantage of our protocol is the ability to generate catalytically favorable mesopore features on the surfaces of our products, due to volume shrinkage in proceeding from TMO to TMN, via a high-temperature annealing step.[9]

In terms of relevant prior work, it was previously reported that W₂N₃ could be obtained by annealing hexagonal-phase tungsten oxide within an ammonia atmosphere; such a process had been used to generate cracked nanosheet motifs.[10] Nevertheless, according to previous studies, only two-dimensional (2D) motifs of W₂N₃ structures (i.e., plates and nanosheets) have been generated using this procedure. Whereas 2D materials (such as graphene) possess interesting structure-dependent opto-electronic and catalytic properties, these desirable 2D motifs unfortunately tend to aggregate, because of attractive van der Waals interactions between adjacent planes. This is a serious, practical issue, because spatially well-dispersed samples are

often needed to reliably incorporate and take advantage of 2D materials within the context of functional, macroscopic-scale devices.[11]

Therefore, in this study, we have synthesized morphologically well-defined motifs of hexagonal-phase WO₃, itself prepared by a hydrothermal reaction, as an initial intermediate. As an interesting synthetic modification, it should be noted that K⁺ was introduced into the reaction mixture during the hydrothermal process. The presence of that cation likely assisted in the formation of three-dimensional, flower-like W₂N₃ motifs during the annealing procedure, because K⁺ has previously been reported to enable the growth of 'flower-like' WN.[12] Hence, by constructing a novel 3D flower-like motif of W₂N₃ incorporating 2D sheets as basic building blocks, we not only promote overall structural stability but also retain the favorable, interesting, and inherently unique properties of 2D materials.

We have tested the relevance and activity of our tungsten nitrides in the context of a number of significant electrocatalytic reactions including HER and the CO₂ reduction reaction (CO₂RR). It is worth recalling that electrochemical water splitting proceeds via HER at the cathode, and involves the breakage of water molecules to form hydrogen gas. By contrast, CO₂RR represents a means in which CO₂ can be converted into useful, value-added carboncontaining species at the cathode.

Hence, a key motivation for investigating tungsten nitrides herein has been the idea of replacing conventional catalyst and support materials with potentially novel systems evincing higher efficiency, lower cost, and greater selectivity.[13-15] In particular, the problems with conventional Pt–based catalysts used for these processes not only center on their relatively low abundance and high cost but also revolve around their tendency to either aggregate or contaminate during the actual electrocatalytic reactions themselves. Moreover, whereas carbon

(in its many formulations, such as carbon black, graphene, and carbon nanotubes) is commonly used as an underlying support material, due to its excellent electronic conductivity and high surface area,[16] it can also unfortunately easily oxidize, thereby resulting in issues associated with poor durability and stability.

As mentioned earlier, tungsten nitride does indeed evince reasonable activity as a functional electrocatalyst. Specifically, within the family of various WN_x materials, the one incorporating a 1: 1 ratio of W to N demonstrated promise as an effective HER, ORR, and MOR catalyst. Furthermore, W₂N was also found to be a decent ORR catalyst, and its performance was enhanced in the context of W₂N/reduced graphene oxide composites.[17] By contrast, W₂N₃ has only been reported as an HER catalyst in one instance.[6] From this limited prior literature, it is evident that though tungsten nitride can inherently give rise to potentially good activity, however, its measured activity alone is not necessarily comparable with that of precious metals such as Pt.

Hence, as a promising strategy with which to improve the electrocatalytic performance of tungsten nitrides, we have deposited relatively small amounts of precious metals (i.e., Pt and Au) onto their external surfaces. The reasoning behind this strategy is that a relatively low loading of precious metals immobilized onto an underlying nitride platform would not only be cost-effective but also induce a reasonable and comparable measured activity (due to beneficial, synergistic metal – metal nitride interactions) with respect to pure precious metal catalysts alone.

Accordingly, in our experiments herein, in terms of describing our *catalytic advances* herein, we have predicted and found that (i) our nitrogen-rich, three-dimensional, flower-like W₂N₃ motifs would exhibit excellent activity towards HER under both alkaline and acidic conditions.[2, 18] (ii) Second, with respect to CO₂ reduction, to the best of our knowledge, the intrinsic performance of tungsten nitride has not been reported thus far, mainly because tungsten

nitride possesses an inherently high activity towards HER, which directly competes with CO₂ reduction. Hence, in this context, our findings are clearly interesting and novel for this reaction. Moreover, an analogue of tungsten nitride, i.e. tungsten carbide, has previously been studied as a support for several transition metals in the context of CO₂ reduction.[19] However, the use of tungsten carbide was reported to suffer from issues emanating from corrosion and instability under neutral and alkaline environments.[20] Hence, we have demonstrated that tungsten nitride may represent a reasonably stable support for deposited, immobilized precious metals for the CO₂ reduction reaction. Furthermore, in an attempt to broaden the functional flexibility and scope of our as-prepared materials within the context of electrocatalytic reactions, we have tested not only the performance but also the stability of our W₂N₃ materials by creating composite catalysts in which Pt was deposited onto the underlying nitride surface in the context of MOR. The data associated with this set of experiments are presented in the SI section.

Overall, we should *emphasize* that our novel *synthetic advances* presented in this paper have included the production of not only (i) novel, nitrogen-enriched three-dimensional (3D) micron-scale flower-like motifs of W₂N₃ composed of constituent two-dimensional nanosheets but also (ii) Pt/W₂N₃ and Au/W₂N₃ composite catalysts, constructed by directly depositing small and well-dispersed Pt or Au nanoparticles onto as-prepared W₂N₃ flower-like aggregates with controlled metal loading amounts. The latter have been subsequently applied toward CO₂RR, as a possible means of enhancing electrocatalytic activity, stability, and selectivity.

2. Experimental section

2.1. Synthesis of Tungsten nitride flower-like motifs

In order to synthesize the nitrogen-rich phase of W_2N_3 , we needed to generate hexagonal WO₃ as precursors. Specifically, 0.577 g sodium tungstate dihydrate (Na₂WO₄•2 H₂O, Sigma BioUltra, $\geq 99.0\%$) and 0.0767 g potassium sulfate (K₂SO₄, Baker Chemical, 99.9%) were dissolved in 10 mL deionized (DI) water by magnetic stirring for 5 minutes so as to form a transparent solution. Subsequently, different amounts of 3.0 M hydrochloric acid (HCl, volume = 0.75 mL, 1.0 mL, 1.25 mL, 1.5 mL, and 2.0 mL, Fisher Scientific, NF/FCC Grade) were added into the above mixture dropwise, until the mixture color had turned into a milk-white hue. Then this homogenous suspension was subsequently transferred to a 25 mL stainless steel autoclave, which was held at a temperature of 180°C for 12 hours. Thereafter, the resulting light-blue products were isolated by centrifugation, and then washed with both water and an ethanol reagent (VWR Chemicals, 95% purity for washing purposes) for several times. After the resulting powder product was dried under vacuum, it was annealed in argon at 450 °C for 3 hours. We then switched the gas to a more reductive 100% ammonia composition, heated the mixture to 700°C with a ramping rate 2°C min⁻¹, and held it for 3 hours under an NH₃ flow of 125 sccm. Eventually, a black tungsten nitride powder was obtained, after the tube furnace was cooled down to room temperature and flushed with Ar, prior to the sample's removal.

2.2. WN particle synthesis

WN powders used as the control sample in HER experiments were prepared from a tungsten (VI) chloride (99.99%) precursor (Sigma Aldrich). The synthesis procedure used was adapted from a prior reported protocol.[21] Specifically, these metal chloride powders were added to 100 mL of chloroform (>99.5%, Sigma Aldrich) to which 100% ammonia (99.995%, Praxair Distribution) was continuously bubbled in until the chloroform had completely evaporated. Then the powders were transferred to a quartz boat, which was subsequently inserted

into a horizontal quartz tube furnace. Thereafter, the reaction was initiated by introducing 100% ammonia at ambient pressure, which was flowed in at 150 sccm. The furnace was ramped from room temperature to 700°C at a rate of 2°C min⁻¹. Then the temperature was held at 700°C for 4 h. Ultimately, the furnace was cooled to room temperature under an NH₃ flow, and then purged with argon gas, prior to sample removal from the furnace.

2.3. Precious metal deposition

2.3.1. Platinum NPs on Tungsten Nitride Nanosheets

Platinum nanoparticles have been deposited onto tungsten nitride microflower motif via a simple, rapid, and relatively non-destructive direct deposition method.[22] Specifically, to prepare specific weight percentages of relatively small Pt nanoparticles deposited onto tungsten nitride, 30 mg of well-ground tungsten nitride powder was dispersed in 30 mL DI water with sonication for 5 minutes so as to form a homogeneous mixture. As an illustrative example, an initial quantity of hexachloroplatinic acid hydrate (H₂PtCl₆•6 H₂O, Alfa Aesar, 99.9%) solution with a concentration of 0.2 wt.% was added to the tungsten nitride dispersion with magnetic stirring. The above mixture was subsequently stirred for 15 min; then 30 mL of a sodium borohydride (NaBH₄, 0.05 M, Alfa Aesar, 98% powder) solution was added in slowly. After reacting for 2 hours, the resulting black products were collected by centrifugation, washed with water and ethanol for three times, and finally dried under vacuum. Following the same type of protocol, composites created by depositing 5 wt. % Pt and 1 wt.% Pt onto tungsten nitride were also correspondingly synthesized.

2.3.2. Gold NPs on Tungsten Nitride Nanosheets

The procedure involving gold nanoparticle deposition onto tungsten nitride was similar to that of the analogous platinum deposition process, as described in the previous section. Briefly,

30 mg well-ground tungsten nitride powder was dispersed in 60 mL DI water by sonication. At the same time, as an illustrative example, a gold precursor solution was prepared in which a small quantity of gold(III) chloride (AuCl₃, Alfa Aesar, 64.4%) with a concentration of 0.2 wt.% was dissolved within 10 mL of DI water, so as to form a resulting 0.25 mM precursor solution. Thereafter, small amounts of gold precursor solution were quickly added into the tungsten nitride dispersion with vigrous magnetic stirring. After 10 min of reaction, the sample was isolated by centrifugation and washed with water in order to remove any remaining Au precursor. Using the identical methodology, the corresponding 5 wt.% and 10 wt.% Au-tungsten nitride composite samples were synthesized.

2.4. Characterization

2.4.1. X-ray diffraction

Powder X-ray Diffraction (XRD) patterns were used to confirm both the sample composition and crystallinity. Specifically, the tungsten nitride sample was initially dispersed in an ethanol solution and then deposited onto a zero background holder (MTI Corporation, Zero diffraction plate for XRD, B-doped, p-type Si, 23.6 mm in diameter by 2 mm in thickness) prior to drying in air. The XRD pattern was obtained using a Rigaku Miniflex diffractometer in the range of 10° to 80° with a scanning rate of 15° min⁻¹.

2.4.2. Scanning electron microscopy

Data on the morphology and size of the as-prepared sample were acquired by means of scanning electron microscopy (SEM). The SEM sample was prepared by depositing aliquots of the sample dispersion in question in ethanol onto a silicon wafer following by drying in air, prior to characterization with a Hitachi 4800S instrument.

2.4.3. Transmission electron microscopy

With the aim of not only verifying the presence of but also characterizing the particle size and distribution of as-deposited precious metal particles, transmission electron microscopy (TEM) was utilized. In preparing the TEM sample, a dilute sample dispersion in ethanol was initially prepared by sonication. Subsequently, an aliquot of the sample was dropped onto a carbon-coated copper grid and dried in air. The TEM image was taken using a JEOL 1400 LaB6 TEM instrument, operating at an accelerating voltage of 120 kV and equipped with a 2048 × 2048 Gatan CCD camera. To obtain precise lattice and crystallographic information, high-resolution TEM (HRTEM) images were obtained as well using a JEOL 2100F instrument, running with an accelerating voltage of 200 kV.

2.4.4. X-ray photoelectron spectroscopy

X-ray photoelectron spectroscopy (XPS) was used to determine the elemental composition of the as-prepared sample and to study the valence states of different elements on the sample surface. Specifically, the XPS sample was prepared by depositing the sample dispersion onto a silicon wafer (measuring 1 cm \times 1 cm). The characterization process was conducted using a home-built XPS system with Al K α radiation (1486.6 eV) as the X-ray source, using the SPECS Phoibos 100 electron energy analyzer as the electron detector.

2.4.5. Electrochemical characterization

1. Hydrogen evolution reaction (HER)

A three-electrode system was constructed in order to evaluate the HER performance. Accordingly, different electrolytes, namely 0.5 M H₂SO₄ and 0.1 M KOH, were prepared for the purposes of creating acidic and basic environments, respectively. These concentrations were typically chosen to simulate the environment within either acidic proton exchange membrane or alkaline anion exchange membrane cells, respectively. The counter electrode consisted of

graphite paper, and the reference electrode was a saturated calomel electrode. The working electrode was prepared immediately prior to the measurements themselves. The catalyst ink was drop cast onto a glassy carbon electrode and subsequently air dried, prior to testing. Specifically, an ink with a concentration of 2 mg mL $^{-1}$ was prepared by dispersing catalysts into a 50/50 (v/v) isopropanol and water solution, containing 0.5 wt. % Nafion as the binder, in order to render a final catalyst concentration of 2 mg mL $^{-1}$. The total catalyst loading on the 5 mm glassy carbon disks was 30 μ g. Once the cell was constructed, catalysts were repeatedly scanned, until the profiles of successive cyclic voltammetry (CV) scans were stabilized and could be replicated in a process that typically lasted 20 scans. These CVs were used to equilibrate samples after being stored in air, and these data were acquired between the range of 0.05 and 0.5 V vs RHE. Thereafter, linear sweep voltammetry (LSV) scans were swept from 0 to -0.7 V (vs. RHE) for the HER measurements.

2. CO_2 reduction reaction

The electrochemical CO₂ reduction performance was assessed using a three-electrode system with an H-shaped cell, consisting of two chambers separated by a Nafion 117 membrane. The electrolyte was prepared by bubbling CO₂ gas into a 0.25 M sodium carbonate (Na₂CO₃, 99.999%, Sigma Aldrich) solution for 12 hours so as to create a resulting 0.5 M sodium bicarbonate (NaHCO₃) solution with a final pH measured at 7.35. The cell was filled almost to the top with this electrolytic solution, with a remnant gap of ~12 mL. To prepare the corresponding working electrode, appropriate quantities of catalysts were dispersed into an isopropanol solution, containing 0.5 wt. % Nafion as the binder, so as to render a final catalyst concentration of 2 mg mL⁻¹. After sonication, the homogeneous catalyst ink was deposited onto the carbon paper. The working electrode and reference electrode (saturated calomel electrode)

were placed into the cathodic chamber of the reaction cell, whereas the corresponding counter electrode (graphite) was inserted into the anodic chamber.

The working electrode was cycled for 10 cycles between 0.05 to 1.20 V (vs. RHE). After this process, LSV curves were obtained by scanning the working electrode from 0 to -1.2 V (vs. RHE) with a scan rate of 100 mV sec⁻¹ until a reproducible signal was acquired. Subsequently, five additional CV scans were collected from a range of 0.05 to 1.20 V (vs. RHE) while under CO₂ bubbling conditions, so as to remove any products generated during the previous LSV scan. To evaluate the catalysts' performance, the working electrode was held at each constant voltage condition, in a process otherwise known as, chronoamperometry, for a period of 20 min. Before conducting each CO₂ electrolysis run, the reference electrode was calibrated by using a hydrogen electrode (Hydroflex, EDAQ). Upon completion of the CO₂ electrolysis reaction, the products of CO₂RR were analyzed by using a gas chromatography (GC, Agilent, 7890B) instrument, equipped with two columns (Plot-Q and Molsieve), a thermal conductivity detector (TCD), and a flame ionization detector (FID), respectively. The gas was examined internally within the GC apparatus itself. The GC was calibrated by using standard gases (Airgas), containing components such as but not limited to CO (5%), H_2 (2.7%), methane (5%), and ethane (5%). 100 μ L of the as-produced gas was collected from the empty space of the cathodic chamber and injected into the gas chromatography to quantify the resulting gas products. The cell was then re-opened, bubbled in with CO₂, sealed, and taken to the next potential for the CO₂RR.

The calculation of the Faradic efficiency and the current density are provided below. [23-25] The Faradaic efficiency of CO (FE_(CO)) was calculated with the following equations (1) - (4): $N_{(CO)}(in \ gaseous \ phase) = C_{(CO)}(\%) \times 12(mL)/22.4(L \ mol^{-1})$ (1)

 $N_{(CO)}(dissolved\ in\ electrolyte) = K_{(CO)} \times 60(mL) \times 1(g\ mL^{-1})/18(g\ mol^{-1}) \times C_{(CO)}(\%)$ (2)

$$N_{(CO)}(total) = N_{(CO)}(in \ gaseous \ phase) + N_{(CO)}(dissolved \ in \ electrolyte)$$
 (3)

$$FE_{(CO)}(\%) = 2 \times 96485(C \ mol^{-1}) \times N_{(CO)}(total) \times 100 / \int_0^t idt$$
 (4)

 $N_{(CO)}$ (in gaseous phase) represents the CO amount within the empty headspace (12 mL) at the cathodic compartment of the cell. $N_{(CO)}$ (dissolved in the electrolyte) denotes the CO amount dissolved in the catholyte (60 mL), assuming that the dissolved amount obeys Henry's law. The constant $K_{(CO)}$ refers to the molar solubility (1.774 × 10⁻⁵) of CO in water at room temperature. $C_{(CO)}$ is associated with the concentration (%) of CO in the empty headspace, which is determined from the GC analysis. For the $FE_{(CO)}$ calculation, the Faraday constant (96485 C mol⁻¹) and the number of electrons (2) for a single CO production were used. The *i* and *t* parameters are the current (A) and electrolysis time (s), as measured by the chronoamperometry technique. The same procedure was used for calculating the FE of H_2 (FE_(H2)), except for its different molar solubility in water (i.e., $K_{(H2)} = 1.411 \times 10^{-5}$).

The total current density $(J_{(total)})$ and the partial current densities of CO $(J_{(CO)})$ and H_2 $(J_{(H2)})$ were calculated, based on the following equations (5) - (7):

$$J_{(CO)}(mA\ cm^{-2}) = FE_{(CO)} \times \int_0^t idt/A/100$$
 (5)

$$J_{(H2)}(mA cm^{-2}) = FE_{(H2)} \times \int_0^t idt/A/100$$
 (6)

$$J_{(total)}(mA cm^{-2}) = \int_0^t idt/A/100$$
 (7)

Herein, A represents the geometric area of the working electrode. Most of the error bars within the FE and J calculations were within 3%, a finding which was attributed to the repeated gas analyses needed to obtain reliable gas composition data.

3. Results and Discussion

3.1. Synthesis of Tungsten Nitride (W₂N₃) and its Composites with Precious Metals

3.1.1. Tungsten nitride (W₂N₃) Synthesis

The synthesis of W₂N₃ was accomplished using an initial hydrothermal reaction, followed by annealing in Ar and NH₃ at high temperature for several hours so as to incorporate nitrogen atoms within an underlying tungsten lattice. As previously reported, a high-temperature ammonia annealing process is capable of introducing nitrogen atoms within a hexagonal WO₃ (*h*-WO₃) lattice, thereby forming a nitrogen-rich phase of W₂N₃.[10] The isolation of a tungsten oxide phase with its corresponding morphology is highly pH-dependent, implying the significance of the precursor solution in affecting the resulting product shape and composition.[26]

In order to obtain a pure *h*-WO₃ precursor, the pH was controlled by adjusting the HCl amounts within the context of the hydrothermal reaction medium. Five different HCl amounts (i.e., 0.75 mL, 1.0 mL, 1.25 mL, 1.5 mL, and 2.0 mL, respectively) were tested. After 12 hours of hydrothermal reaction at 180°C, the XRD patterns of the resulting products are shown in Figure S1, Figure 1A, and Figure S2, respectively. When the introduced HCl volume was set at 0.75 mL, W₁₈O₄₉ was generated (Figure S1). When that HCl volume was increased to 1.0 mL, hexagonal tungsten oxide was generated, as suggested by the XRD pattern shown in Figure 1A. Indeed, the positions of the tungsten oxide peaks match well with those of the standard XRD pattern (corresponding to JCPDS No. 75-2187) without any obvious impurities, a finding indicative of the formation of pure hexagonal WO₃. With a further increase in the amount of HCl,

a pure orthorhombic phase of tungstate (*o*-WO₃ • 0.33 H₂O) in addition to mixed phases of tungsten oxide could be generated, as shown in Figure S2.

Figure 1B highlights the XRD pattern of an as-prepared tungsten nitride sample; its peaks correspond well with those of the calculated hexagonal-W₂N₃ (h-W₂N₃) standard diffraction pattern, as reported by Wang et al., with no detectable impurities present. [7] In addition, XPS has been used for elemental composition analysis; the results are shown in Figure 1C and 1D. The survey spectrum of W₂N₃ present in Figure S3 shows the presence of all of the peaks associated with W, N, C, and O with no apparent impurity, except for the Na 1s peak, which likely originated from the tungsten precursor Na₂WO₄ used in the hydrothermal process. Figure 1C depicts the nitrogen 1s scan, which highlights two peaks located at 398.5 eV and 400.1 eV. The first peak can be ascribed to the tungsten-nitrogen bond, whereas the second one can be assigned to the nitrogen atoms near the nitrogen vacancies. [6, 27, 28] There are four peaks which can be found in the tungsten 4f scan in Figure 1D; these are located at 38.7 eV, 36.6 eV, 36.0 eV, and 33.9 eV, respectively. In particular, the peaks at 38.7 eV and 36.6 eV can be assigned to W $4f_{5/2}$ and W $4f_{7/2}$, respectively, indicative of tungsten-oxygen interactions, owing to the partial oxidation on the surface. The peaks situated at 36.0 and 33.9 eV correspond to characteristic W $4f_{5/2}$ and W $4f_{7/2}$ signals, emanating from tungsten-nitrogen bonds. According to the XPS peak area and the corresponding sensitivity factor, the resulting measured atomic ratio between W and N is 1: 1.18, which is lower as compared with the stoichiometry of W_2N_3 (W: N = 1: 1.5). This finding is likely indicative of the presence of nitrogen vacancies within as-prepared h-W₂N₃, and agrees well with the N 1s results. In addition, XPS only provides the elemental information originating from the topmost ~10 nm of the sample surface; hence, this low measured amount of N could also potentially be ascribable to partial surface oxidation.

The morphology of the as-obtained tungsten oxide immediately after the hydrothermal reaction consisted of nanorods, as shown in Figure S4. Upon high-temperature annealing, micron-scale flower-like structures of W₂N₃ were generated, as shown in Figure 2. Indeed, the SEM and TEM images depict flower-like motifs, possessing average diameters of 3~5 µm and composed of constituent two-dimensional nanosheets. The morphological transformation from tungsten oxide nanorods to tungsten nitride micron-scale flowers could likely be attributed to the mediation of K⁺ from K₂SO₄. Indeed, nanosheets likely formed, due to K⁺ adsorbing onto the specific facets of growing tungsten oxide nanorods and facilitating the concomitant growth of perpendicular structures, during the high-temperature annealing process.[12]

3.1.2. Platinum/Tungsten nitride

Through a facile direct deposition process, varying amounts of Pt nanoparticles were immobilized onto the underlying tunsgten nitride nanosheets. Figure 3 highlights the formation of a series of Pt/W₂N₃ composites with varying amounts of Pt loading from 1 wt. %, 5 wt. %, to 10 wt. %. Figure 2D depicts bare W₂N₃ nanosheets, which clearly do not show any presence of particles. When Pt was deposited with different loading amounts, the Pt nanoparticles were uniformly dispersed onto the nanosheets, as shown in Figure 3A, 3B, and 3C. Moreover, with increasing Pt content, the Pt particle sizes augmented somewhat as well. Specifically, the sizes of Pt rose from 1.53 nm with 1% Pt loading, to 2.27 nm with 5% Pt loading, and finally to 3.01 nm with 10% Pt loading onto the underlying W₂N₃ platform. Quantitative data concerning the relevant Pt nanoparticles' size and distribution are summarized in Figure S5 and Table S1. Indeed, we found that the Pt particle size increases proportionally with a corresponding increase in the Pt precursor amount, an observation consistent with a prior report. [29]

HRTEM images of composites created from Pt/W₂N₃ with various Pt loadings are presented in Figure 3D, E, and F. The lattice fringes of the platinum nanoparticles were measured to be 0.230 nm, 0.230 nm, and 0.231 nm, corresponding to Pt sample loadings of 1%, 5%, and 10%, respectively. These data could be related to a lattice expansion of the Pt(111) plane, due to tension-induced strain emanating from depositing Pt onto the underlying substates, a phenomenon corroborated by previous work.[30] In addition, the lattice distances of W₂N₃ were measured and found to be 0.250 nm, 0.249 nm, and 0.250 nm, respectively, for these three samples, a finding that matched well with lattice distances associated with the (100) plane. The corresponding Fast Fourier Transform (FFT) patterns were inserted as insets into the image of Figure 3 as well, highlighting the presence of two different, distinctive phases within the characterized region; these data could likely be ascribed to the formation of both Pt and W₂N₃, in a manner consistent with the expected formation of the metal/metal nitride-based heterostructure.

3.1.3. Gold/Tungsten nitride

The Au/W₂N₃ samples were successfully synthesized using a similar method for the analogous Pt/W₂N₃ composites. According to the 'metal activity sequence', the positively charged gold cation (Au³⁺) should be comparatively easier to reduce to its corresponding neutral gold metal formulation as compared with the analogous process of converting multi-valent platinum ions (PtCl₄²⁻) to Pt itself. Therefore, in our synthesis protocol, no reducing agent was used. From the prior literature,[31, 32] the relatively facile spontaneous reduction of Au cations enabled the deposition of Au onto not only both WS₂ and MoS₂ nanosheets but also carbon-based materials as well. Indeed, these processes were reported to have arisen from and to have been facilitated by a charge transfer phenomenon, occurring between either transition metal dichalcogenides or carbon-based materials to the adjacent gold ions, thereby leading to Au

nanoparticle formation.[31, 32] Considering the unique nature of the reduction process of Au³⁺, it was found that the use of a greater concentration of tungsten nitride generally correlated with a correspondingly larger gold nanoparticle size, wherein the Au loading amounts were the same, as shown in Figure 4.

Indeed, in (i) the absence of any additional reducing agent and by (ii) running the deposition treatment for 10 min at room temperature, three different 10 wt.% Au / tungsten nitride composites incorporating three distinctive Au sizes were synthesized by using various concentrations of a W₂N₃ dispersion, namely 1.0 g L⁻¹, 0.5 g L⁻¹, and 0.1 g L⁻¹. What is worth mentioning is the relatively homogeneous distribution of Au NPs noted, regardless of the loading levels tested. When the concentration of the W₂N₃ dispersion was 1.0 g L⁻¹, relatively large nanoparticles possessing an average diameter of ~30.5 nm were uniformly dispersed onto the underlying tungsten nitride nanosheet, as shown in Figure 4C. With a halving of the W₂N₃ precursor solution concentration to 0.5 g L⁻¹, diameters of Au particles correspondingly decreased to 10.1 nm (Figure 4B). Interestingly, the Au size increased slightly to 12.8 nm with a further reduction in the initial W₂N₃ concentration to 0.1 g L⁻¹ (Figure 4A). Similarly, in a parallel series of runs, by using a 0.5 g L⁻¹ W₂N₃ solution with which to prepare Au/tungsten nitride composites, the analogous, as-synthesized 5 wt.% Au/tungsten nitride heterostructures, shown in Figure 4D, incorporated individual average Au nanoparticles measuring ~7.5 nm in terms of average diameter. As implied, our findings highlight that deliberative changes in the precursor concentration during the reduction process correlated with the resulting Au nanoparticle size, distribution, and density observed, as shown in Figure S6 and Table S2.

3.2. Electrochemical Catalysis of Tungsten Nitride and its Composites

3.2.1. Hydrogen evolution reaction (HER)

The catalytic activity of W₂N₃ as HER catalysts was evaluated in both acidic and alkaline environments, using a three-electrode system. In addition, in order to assess the comparative HER performance of as-prepared W₂N₃, WN particulate powder was also tested under the same conditions as a control sample. The polarization curves associated with the WN control sample and as-prepared micron-scale flower-like motifs of W₂N₃ within both acidic (0.5 M H₂SO₄) and alkaline (0.1 M KOH) environments are shown in Figure 5A and 5B.

When the electrochemical measurements were performed under acidic conditions, as highlighted in Figure 5A, W₂N₃ was found to have exhibited a catalytically desirable, significantly lower overpotential value as compared with the use of WN. Specifically, the measured overpotential values, necessary to achieve a current density of 10 mA/cm², were found to be -101 mV (vs. RHE) for W₂N₃ and -658 mV (vs. RHE) for WN. By analogy, the corresponding electrochemical test results obtained under an alkaline environment are shown in Figure 5B. Indeed, the overpotential value for W₂N₃ (i.e., -481 mV vs. RHE) was improved as compared with WN (i.e., -538 mV vs. RHE). In addition, the onset potential of as-prepared W₂N₃ was measured to be lower as compared with that associated with the control sample of WN in both acidic and alkaline environments. All of these results are presented in Table 1. Hence, according to this set of electrochemical measurements, the as-prepared W₂N₃ samples gave rise to better electrocatalytic activity within the HER process as compared with WN alone under both acidic and alkaline environment conditions, thereby reinforcing the notion of an intrinsically higher catalytic performance associated with the nitrogen-rich phase of W₂N₃.

To place the electrochemical activity of our as-prepared flower-like W_2N_3 motifs into context, we compared our results with the corresponding catalytic activities of other reported tungsten nitride-based HER catalysts within both (i) acidic and (ii) alkaline environments. That

summary analysis is presented in Tables S3 and S4, respectively. From these data, it is apparent that our as-generated flower-like W_2N_3 samples yielded either comparable or even superior HER performance with respect to existing systems within an acidic medium. By contrast, for the HER process within the corresponding alkaline solution, our sample did not perform as well.

3.2.2 CO₂ Reduction Reaction (CO₂RR)

The CO₂ reduction fundamentally involves converting CO₂ to CO, which becomes a source for useful carbon-containing feedstock.[23] Because HER occurs simultaneously and represents a key competing side reaction, the HER process needs to be suppressed in order to achieve a higher Faradaic efficiency towards CO production. As such, Au is often used in this context, because of its relatively low HER activity and comparatively high selectivity towards CO.[24] Making use of this prior knowledge, we prepared composites, constructed from nitrogen-rich tungsten nitride (W_2N_3) onto which Au nanoparticles of a number of different sizes had been immobilized with various loading amounts, and subsequently assessed their CO₂ reduction performance. Specifically, as implied earlier, by carefully controlling precursor concentrations and amounts used, four different Au/W₂N₃ composite samples, incorporating various loadings of distinctively sized Au NPs, have been generated. These included the following series, described in terms of average weight loadings of immobilized, individual Au NPs with associated measured average diameters: (1) 5% wt. loading with ~7 nm Au NPs; (2) 10% wt. loading with ~13 nm Au NPs; (3) 10% weight loading with ~15 nm Au NPs; and (4) 10% wt. loading with ~30 nm Au NPs.

The different Faraday efficiency (FE) values associated with the formation of different CO₂ reduction products catalyzed by using these different Au/W₂N₃ composites are highlighted and compared in Figure 6A. For these four Au/W₂N₃ catalysts, all were found to have generated

 H_2 (FE > 95%), as opposed to CO, as a major product at -0.8 V (vs. RHE), thereby suggesting that tungsten nitride is actually a much better HER (as opposed to CO_2RR) catalyst. This finding is also confirmed by the current density results, shown in Figure 6B, indicating that the current densities for CO formation at -0.8 V (vs. RHE) for all of the Au/W_2N_3 composites are lower than 1 mA/cm^2 . The combination of a simultaneously low FE and current density for CO formation confirms the relatively poor CO_2 reduction activity of Au/W_2N_3 composites, which are more inherently disposed toward improved performance for the competing HER process.

By means of comparison, CO₂ reduction reaction results associated with Au/C (20 wt%, E-tek, particle size: 4 nm) are presented in Figure S8. These data with carbon as the support highlighted a much higher Faraday efficiency towards CO as compared with H₂, the precise magnitude of which may have been impacted by the amount of Au loading. Nonetheless, this observed catalytic behavior with the carbon control underscored the significance of the choice of the underlying support material, since the use of W₂N₃ in the guise of Au/W₂N₃ yielded essentially the exact opposite result, namely a much greater H₂ production relative to that of CO.

Nevertheless, what is significant and worth highlighting from our data herein is that the catalytic activity could be controllably tuned to a certain degree through sample composition. Specifically, even though the Au/W_2N_3 composite yielded a poor overall catalytic performance, the measured reaction activities and as-generated CO/H_2 ratios actually depended upon both (i) the Au nanoparticle sizes and (ii) loading quantities, as shown in Figure 6C, though not necessarily in a linearly proportionate and correlative fashion. For example, with Au/W_2N_3 samples incorporating different Au sizes, it was noted that the 13 nm Au/W_2N_3 sample evinced the 'best' relative performance among all of the samples tested. Moreover, it was found that

when decreasing the amount of Au loading, the associated measured CO/H₂ ratio was much smaller with the 5 wt.% composite as compared with their 10 wt.% sample analogues.

According to these cumulative electrochemical measurement data, when using Au/W_2N_3 as CO_2 reduction catalysts, we found that W_2N_3 favors hydrogen evolution as opposed to CO formation under CO_2 reduction conditions. With the mediation of Au nanoparticles immobilized onto the underlying W_2N_3 micron-scale flower-like motifs, small quantities of CO were generated. In addition, the measured CO/H_2 ratio was found to have increased with and correlated with the addition of Au NPs.

4. Conclusions

We have successfully generated three-dimensional flower-like tungsten nitride W_2N_3 composed of nanosheets, via a facile hydrothermal process followed by annealing in argon and NH₃. Indeed, our strategy involves the nitridation of chemically and morphologically well-defined TMO intermediates as a plausible synthetic means for simultaneously and reliably tuning both morphology and chemical composition.

As previously mentioned, it is expected that the electrocatalytic activity emanating from these materials originates from the presence of the nitrogen in the form of W-N bonds. Not surprisingly, as-prepared W₂N₃ evinced reasonable HER activities in both acidic and alkaline environments. Indeed, the measured HER activity of our sample was comparable to that noted previously for W₂N₃ flakes,[6] which is a logical finding considering the high surface-area and structural integrity of our as-prepared materials.

In addition, by using a direct deposition method, we were able to immobilize and anchor Pt nanoparticles with different loading amounts onto W_2N_3 and to subsequently apply these

composites as MOR catalysts. Furthermore, by using a similar strategy, Au nanoparticles were relatively evenly deposited onto an underlying tungsten nitride platform in the absence of a reducing agent; these composites were applied as CO₂RR catalysts. By analogy, we found that the sizes of the as-obtained Au particles could be reliably tuned by correspondingly modifying the tungsten nitride concentration during the synthesis process. Nevertheless, owing to the comparatively higher HER activity of W₂N₃, we noted that our as-prepared Au/W₂N₃ samples preferred to generate H₂ as opposed to CO during the electrochemical process.

5. Supporting Information Available

Additional information on MOR experiments and results; XRD patterns; SEM and TEM data, in addition to complementary XPS characterization data acquired for the samples analyzed.

6. Acknowledgements

This material is based on work performed in SSW's laboratory, supported by the U.S. National Science Foundation under Grant No. CHE-1807640. Structural characterization experiments (TEM, SEM, and XPS) for this manuscript were performed in part at the Center for Functional Nanomaterials, located at Brookhaven National Laboratory, which is supported by the U.S. Department of Energy under Contract No. DE-SC-00112704. Authors from Columbia University acknowledge support from the U.S. Department of Energy, Office of Science, Catalysis Science Program (DE-FG02-13ER16381). BMT acknowledges support from the U.S. Department of Energy, Office of Science, Office of Workforce Development for Teachers and Scientists, Office of Science Graduate Student Research (SCGSR) program. The SCGSR

program is administered by the Oak Ridge Institute for Science and Education for the DOE under contract number DE-SC0014664.

7. Dedication

I was a graduate student in Professor Lieber's laboratory during the 1990s. Charlie continues to be an inspirational role model of what any serious and thoughtful scientist should aspire to be. His profound scientific rigor and curiosity, his unrelenting pursuit of excellence and emphasis on critical thinking, in addition to his persistence, intense dedication, and premium on the value of hard work have guided me ever since. Coupled with his strong and unwavering support, I am eternally grateful to him for truly enabling, in so many different ways, my own successes during my career. I wish him the very best.

References

- [1] Levy, R. B.; Boudart, M. Platinum-Like Behavior of Tungsten Carbide in Surface Catalysis. *Science* **1973**, *181*, 547.
- [2] Jin, H.; Zhang, H.; Chen, J.; Mao, S.; Jiang, Z.; Wang, Y. A general synthetic approach for hexagonal phase tungsten nitride composites and their application in the hydrogen evolution reaction. *Journal of Materials Chemistry A* **2018**, *6*, 10967-10975.
- [3] Yan, H.; Meng, M.; Wang, L.; Wu, A.; Tian, C.; Zhao, L.; Fu, H. Small-sized tungsten nitride anchoring into a 3D CNT-rGO framework as a superior bifunctional catalyst for the methanol oxidation and oxygen reduction reactions. *Nano Research* **2016**, *9*, 329-343.
- [4] Yin, S.; Wang, P.; Lu, J.; Wen, Y.; Luo, L.; Key, J.; Wang, N.; Shen, P. K. Tungsten nitride decorated CNTs as efficient hybrid supports for PtRh alloys in electrocatalytic ethanol oxidation. *International Journal of Hydrogen Energy* **2017**, *42*, 22805-22813.
- [5] Ham, J. D.; Lee, S. J. Transition Metal Carbides and Nitrides as Electrode Materials for Low Temperature Fuel Cells. *Energies* **2009**, *2*, 873-899.
- [6] Yu, H.; Yang, X.; Xiao, X.; Chen, M.; Zhang, Q.; Huang, L.; Wu, J.; Li, T.; Chen, S.; Song, L.; Gu, L.; Xia, B. Y.; Feng, G.; Li, J.; Zhou, J. Atmospheric-Pressure Synthesis of 2D Nitrogen-Rich Tungsten Nitride. *Advanced Materials* **2018**, *30*, e1805655.
- [7] Wang, S.; Yu, X.; Lin, Z.; Zhang, R.; He, D.; Qin, J.; Zhu, J.; Han, J.; Wang, L.; Mao, H.-k.; Zhang, J.; Zhao, Y. Synthesis, Crystal Structure, and Elastic Properties of Novel Tungsten Nitrides. *Chemistry of Materials* **2012**, *24*, 3023-3028.
- [8] Kawamura, F.; Yusa, H.; Taniguchi, T. Synthesis of hexagonal phases of WN and W2.25N3 by high-pressure metathesis reaction. *Journal of the American Ceramic Society* **2017**, *101*, 949-956.
- [9] Peng, X.;Pi, C.;Zhang, X.;Li, S.;Huo, K.; Chu, P. K. Recent progress of transition metal nitrides for efficient electrocatalytic water splitting. *Sustainable Energy & Fuels* **2019**, *3*, 366-381.
- [10] Varga, T.; Haspel, H.; Kormányos, A.; Janáky, C.; Kukovecz, Á.; Kónya, Z. Nitridation of one-dimensional tungsten oxide nanostructures: Changes in structure and photoactivity. *Electrochimica Acta* **2017**, *256*, 299-306.
- [11] Shehzad, K.;Xu, Y.;Gao, C.; Duan, X. Three-dimensional macro-structures of two-dimensional nanomaterials. *Chemical Society Reviews* **2016**, *45*, 5541-5588.
- [12] Zhang, J.; Chen, J.; Yang, H.; Fan, J.; Zhou, F.; Wang, Y.; Wang, G.; Wang, R. Efficient synthesis of nitrogen-doped carbon with flower-like tungsten nitride nanosheets for improving the oxygen reduction reactions. *RSC Advances* **2017**, *7*, 33921-33928.
- [13] Sui, S.; Wang, X.; Zhou, X.; Su, Y.; Riffat, S.; Liu, C.-j. A comprehensive review of Pt electrocatalysts for the oxygen reduction reaction: Nanostructure, activity, mechanism and carbon support in PEM fuel cells. *Journal of Materials Chemistry A* **2017**, *5*, 1808-1825.
- [14] Mahmood, N.; Yao, Y.; Zhang, J.-W.; Pan, L.; Zhang, X.; Zou, J.-J. Electrocatalysts for Hydrogen Evolution in Alkaline Electrolytes: Mechanisms, Challenges, and Prospective Solutions. *Advanced Science* **2017**, *5*, 1700464.
- [15] Vij, V.;Sultan, S.;Harzandi, A. M.;Meena, A.;Tiwari, J. N.;Lee, W.-G.;Yoon, T.; Kim, K. S. Nickel-Based Electrocatalysts for Energy-Related Applications: Oxygen Reduction, Oxygen Evolution, and Hydrogen Evolution Reactions. *ACS Catalysis* **2017**, *7*, 7196-7225.

- [16] Wang, Y.-J.; Wilkinson, D. P.; Zhang, J. Noncarbon Support Materials for Polymer Electrolyte Membrane Fuel Cell Electrocatalysts. *Chemical Reviews* **2011**, *111*, 7625-7651
- [17] Xie, Y.;Zhang, Y.;Zhang, M.;Zhang, Y.;Liu, J.;Zhou, Q.;Wang, W.;Cui, J.;Wang, Y.;Chen, Y.;Wang, Z.;Xie, T.; Wu, Y. Synthesis of W2N nanorods-graphene hybrid structure with enhanced oxygen reduction reaction performance. *International Journal of Hydrogen Energy* **2017**, *42*, 25924-25932.
- [18] Meng, M.; Yan, H.; Jiao, Y.; Wu, A.; Zhang, X.; Wang, R.; Tian, C. A "1-methylimidazole-fixation" route to anchor small-sized nitrides on carbon supports as non-Pt catalysts for the hydrogen evolution reaction. *RSC Advances* **2016**, *6*, 29303-29307.
- [19] Wannakao, S.; Artrith, N.; Limtrakul, J.; Kolpak, A. M. Catalytic Activity and Product Selectivity Trends for Carbon Dioxide Electroreduction on Transition Metal-Coated Tungsten Carbides. *The Journal of Physical Chemistry C* **2017**, *121*, 20306-20314.
- [20] Abbas, S. C.; Wu, J.; Huang, Y.; Babu, D. D.; Anandhababu, G.; Ghausi, M. A.; Wu, M.; Wang, Y. Novel strongly coupled tungsten-carbon-nitrogen complex for efficient hydrogen evolution reaction. *International Journal of Hydrogen Energy* **2018**, *43*, 16-23.
- [21] Choi, D.; Kumta, P. N. Synthesis, Structure, and Electrochemical Characterization of Nanocrystalline Tantalum and Tungsten Nitrides. *Journal of the American Ceramic Society* **2007**, *90*, 3113-3120.
- [22] Qiu, J.-D.; Wang, G.-C.; Liang, R.-P.; Xia, X.-H.; Yu, H.-W. Controllable Deposition of Platinum Nanoparticles on Graphene As an Electrocatalyst for Direct Methanol Fuel Cells. *The Journal of Physical Chemistry C* **2011**, *115*, 15639-15645.
- [23] Sheng, W.; Kattel, S.; Yao, S.; Yan, B.; Liang, Z.; Hawxhurst, C. J.; Wu, Q.; Chen, J. G. Electrochemical reduction of CO2 to synthesis gas with controlled CO/H2 ratios. *Energy & Environmental Science* **2017**, *10*, 1180-1185.
- [24] Lee, J. H.; Kattel, S.; Xie, Z.; Tackett, B. M.; Wang, J.; Liu, C.-J.; Chen, J. G. Understanding the Role of Functional Groups in Polymeric Binder for Electrochemical Carbon Dioxide Reduction on Gold Nanoparticles. *Advanced Functional Materials* **2018**, 28, 1804762.
- [25] Lee, J. H.; Kattel, S.; Jiang, Z.; Xie, Z.; Yao, S.; Tackett, B. M.; Xu, W.; Marinkovic, N. S.; Chen, J. G. Tuning the activity and selectivity of electroreduction of CO2 to synthesis gas using bimetallic catalysts. *Nature Communications* **2019**, *10*, 3724.
- [26] Xu, D.; Jiang, T.; Wang, D.; Chen, L.; Zhang, L.; Fu, Z.; Wang, L.; Xie, T. pH-Dependent Assembly of Tungsten Oxide Three-Dimensional Architectures and Their Application in Photocatalysis. *ACS Applied Materials & Interfaces* **2014**, *6*, 9321-9327.
- [27] Liu, B.; He, B.; Peng, H.-Q.; Zhao, Y.; Cheng, J.; Xia, J.; Shen, J.; Ng, T.-W.; Meng, X.; Lee, C.-S.; Zhang, W. Unconventional Nickel Nitride Enriched with Nitrogen Vacancies as a High-Efficiency Electrocatalyst for Hydrogen Evolution. *Advanced Science* **2018**, *5*, 1800406.
- [28] Jin, H.;Li, L.;Liu, X.;Tang, C.;Xu, W.;Chen, S.;Song, L.;Zheng, Y.; Qiao, S.-Z. Nitrogen Vacancies on 2D Layered W2N3: A Stable and Efficient Active Site for Nitrogen Reduction Reaction. *Advanced Materials* **2019**, *31*, 1902709.
- [29] Grinou, A.; Yun, S. Y.; Cho, Y. S.; Park, H. H.; Jin, H.-J. Dispersion of Pt Nanoparticle-Doped Reduced Graphene Oxide Using Aniline as a Stabilizer. *Materials* **2012**, *5*, 2927-2936.

- [30] Scofield, M. E.; Koenigsmann, C.; Bobb-Semple, D.; Tao, J.; Tong, X.; Wang, L.; Lewis, C. S.; Vukmirovic, M. B.; Zhu, Y.; Adzic, R. R.; Wong, S. S. Correlating the chemical composition and size of various metal oxide substrates with the catalytic activity and stability of as-deposited Pt nanoparticles for the methanol oxidation reaction. *Catalysis Science & Technology* **2016**, *6*, 2435-2450.
- [31] Kim, J.;Byun, S.;Smith, A. J.;Yu, J.; Huang, J. Enhanced Electrocatalytic Properties of Transition-Metal Dichalcogenides Sheets by Spontaneous Gold Nanoparticle Decoration. *The Journal of Physical Chemistry Letters* **2013**, *4*, 1227-1232.
- [32] Shin, H.-J.; Choi, W. M.; Choi, D.; Han, G. H.; Yoon, S.-M.; Park, H.-K.; Kim, S.-W.; Jin, Y. W.; Lee, S. Y.; Kim, J. M.; Choi, J.-Y.; Lee, Y. H. Control of Electronic Structure of Graphene by Various Dopants and Their Effects on a Nanogenerator. *Journal of the American Chemical Society* **2010**, *132*, 15603-15609.

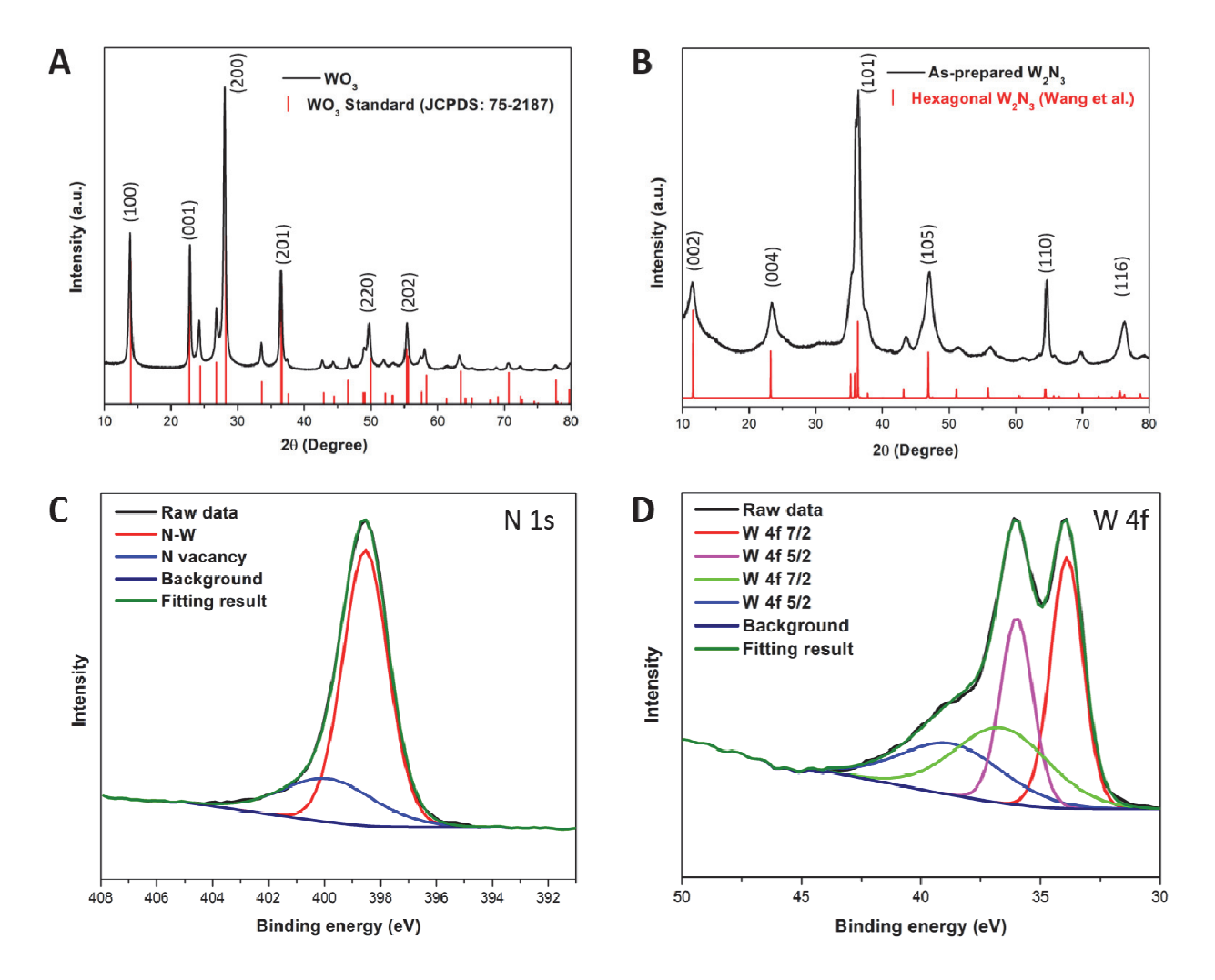


Figure 1. XRD patterns of (A) as-obtained hexagonal WO₃ (black) along with the database standard (JCPDS No. 75-2187) (red), and (B) experimentally-generated W_2N_3 (black) coupled with the calculated diffraction pattern (red) from Wang et al.[7] XPS spectra collected of W_2N_3 and analyzed in the (C) N *1s* range and (D) W *4f* range.

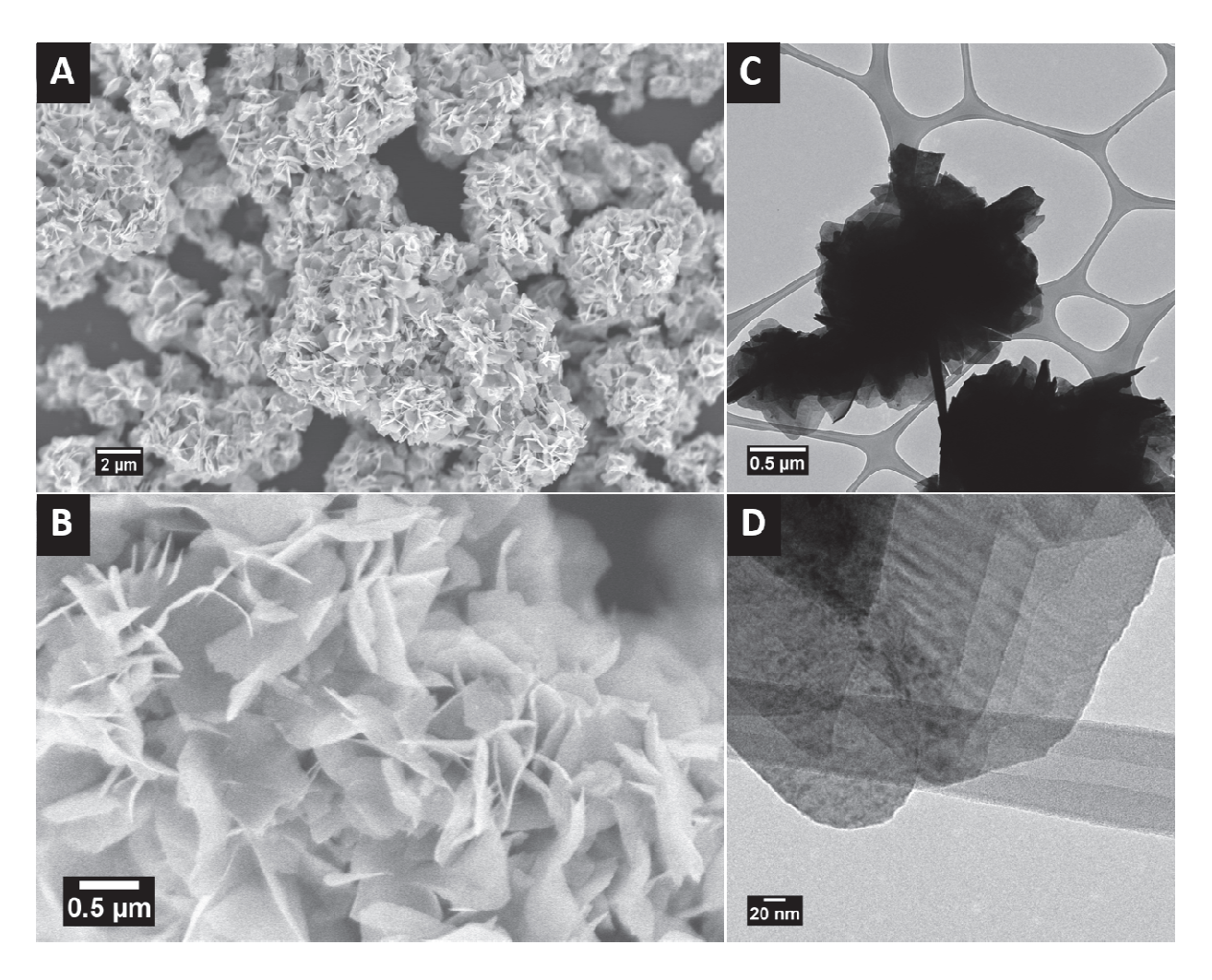


Figure 2. Novelty of Morphology. (A, B) SEM images and (C, D) TEM images of as-prepared, flower-like motifs of W_2N_3 .

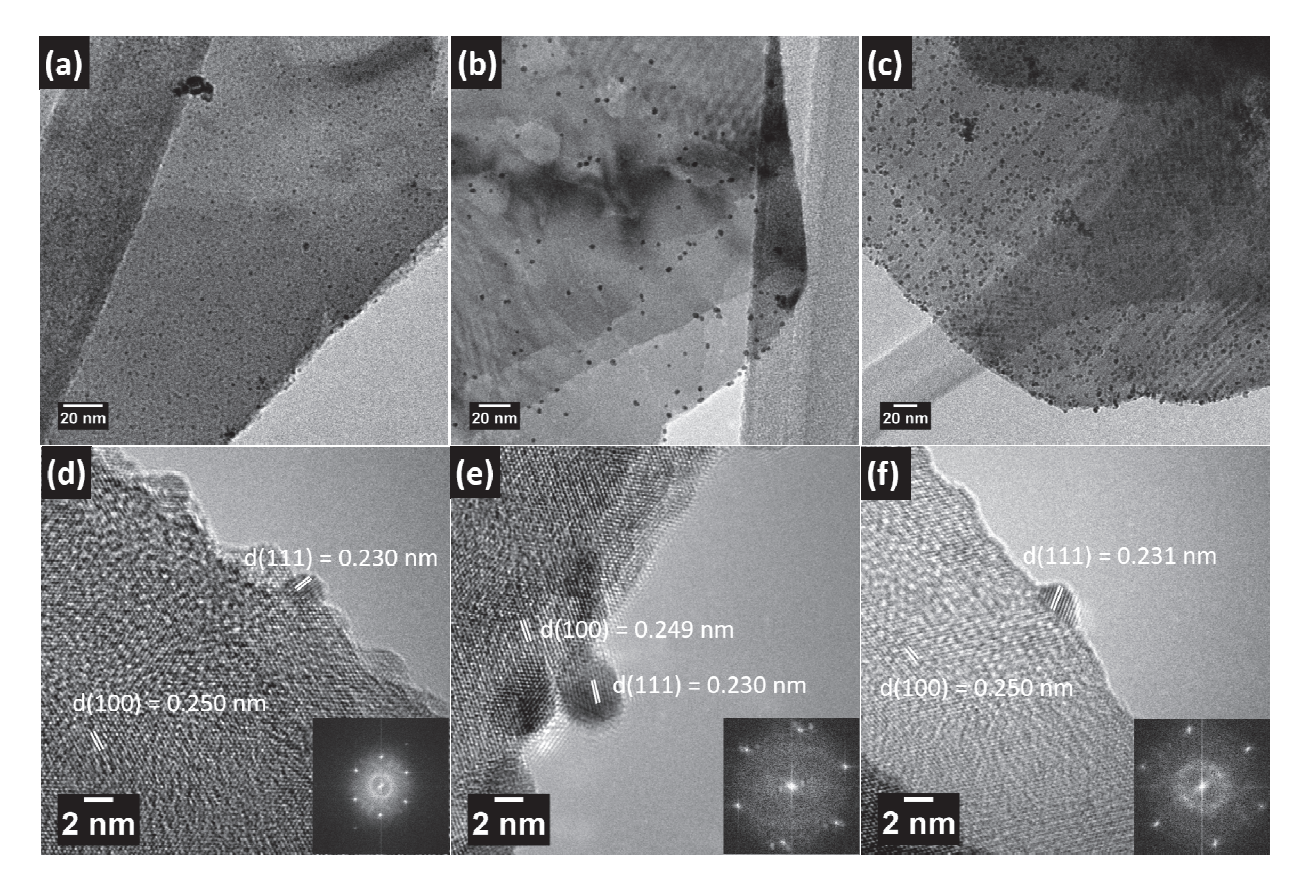


Figure 3. TEM images of Pt/W₂N₃ composites incorporating different Pt loading amounts of (A) 1%, (B) 5%, and (C) 10%, respectively. HRTEM images of Pt/W₂N₃ composites, incorporating different Pt loading amounts of (D) 1%, (E) 5%, and (F) 10%, respectively. Corresponding Fast Fourier Transform (FFT) patterns were inserted in the lower right-hand corners of (D) through (F) as insets.

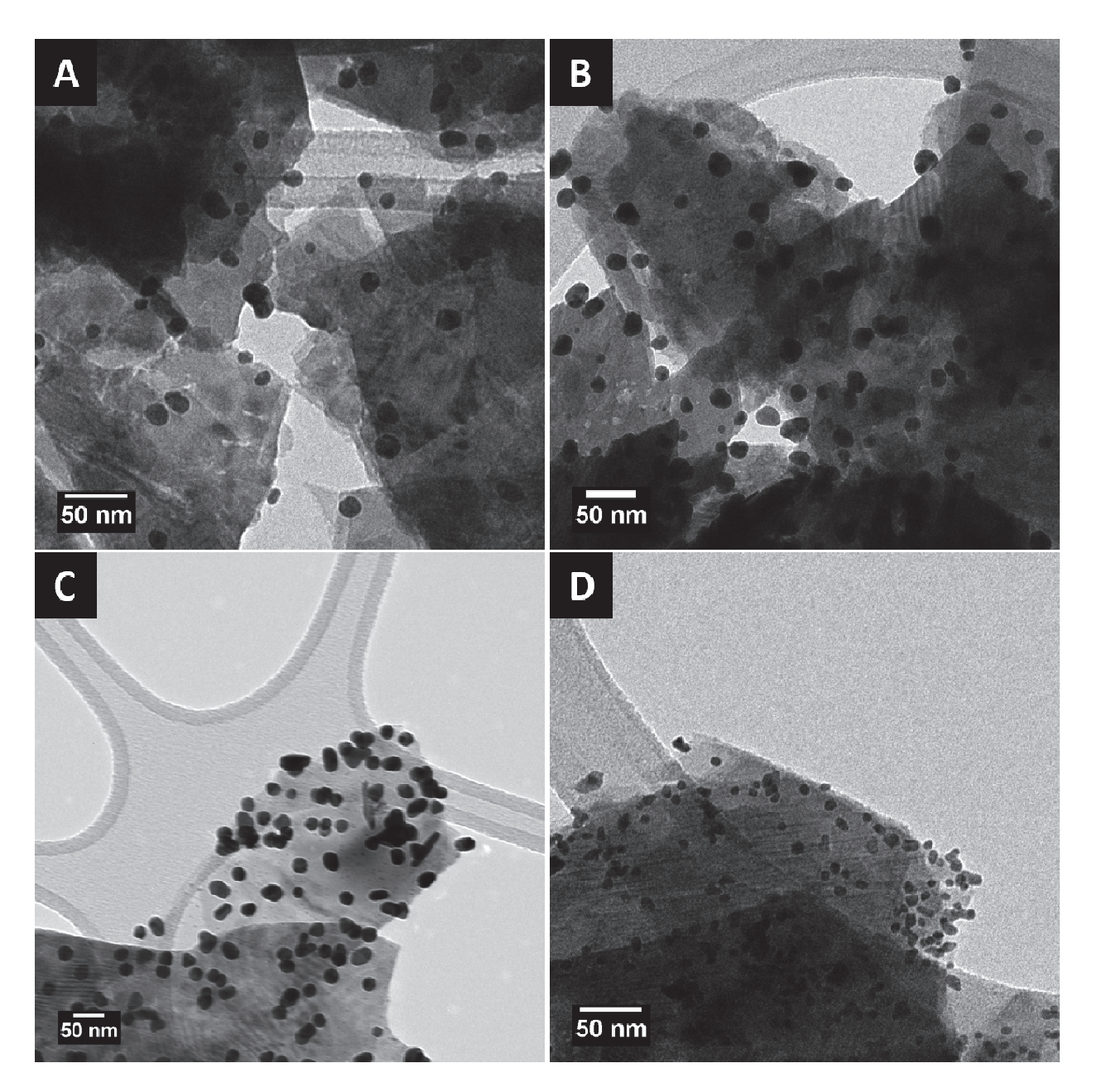


Figure 4. TEM images of composites of Au/W_2N_3 . (A) W_2N_3 concentration: 0.1 g L⁻¹, Au loading amount: 10%; (B) W_2N_3 concentration: 0.5 g L⁻¹, Au loading amount: 10%; (C) W_2N_3 concentration: 1.0 g L⁻¹, Au loading amount: 10%; and (D) W_2N_3 concentration: 0.5 g L⁻¹, Au loading amount: 5%.

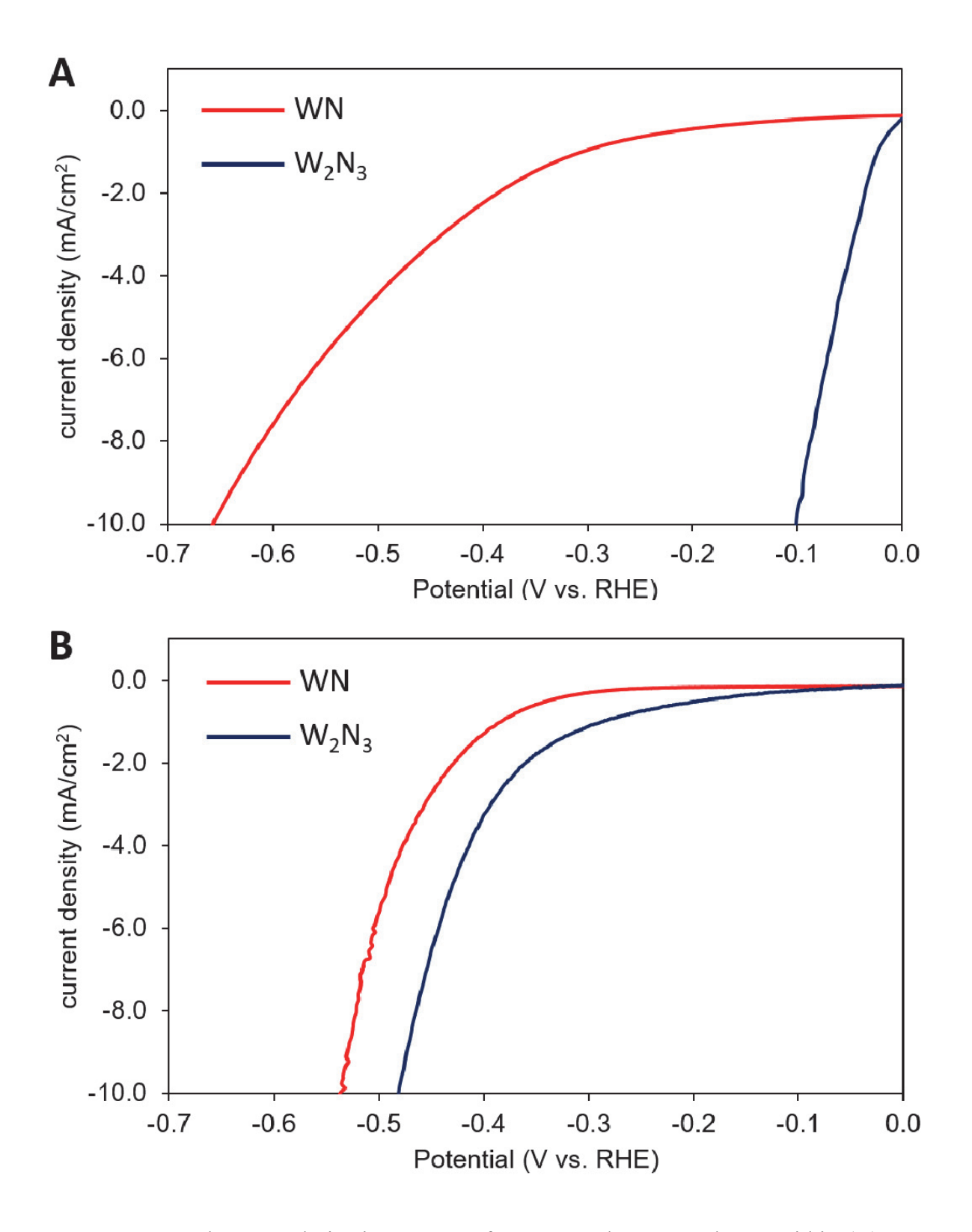


Figure 5. Measured HER polarization curves of as-prepared W_2N_3 and WN within (A) 0.5 M H_2SO_4 solution and (B) 0.1 M KOH solution.

Table 1. Onset potential and η_{10} (the overpotential to achieve a current density of 10 mA/cm²) associated with as-prepared W_2N_3 and WN (control) samples within both acidic and alkaline environments.

Acid electrolyte	Onset potential (mV)	η ₁₀ (mV)
As-prepared W ₂ N ₃	0	-101
WN (control sample)	-31	-648
Alkaline electrolyte	Onset potential (mV)	η ₁₀ (mV)
As-prepared W ₂ N ₃	-14	-482
WN (control sample)	-24	-539

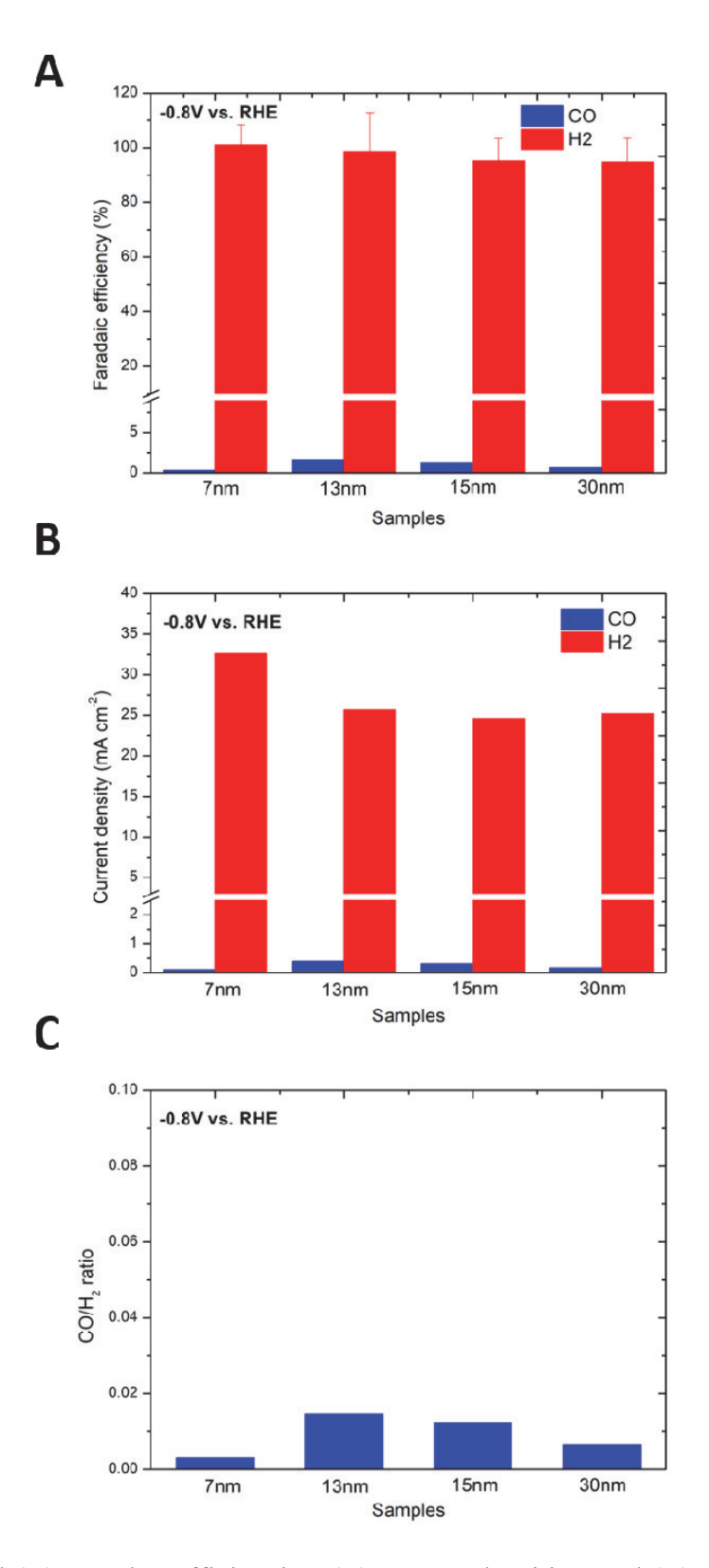
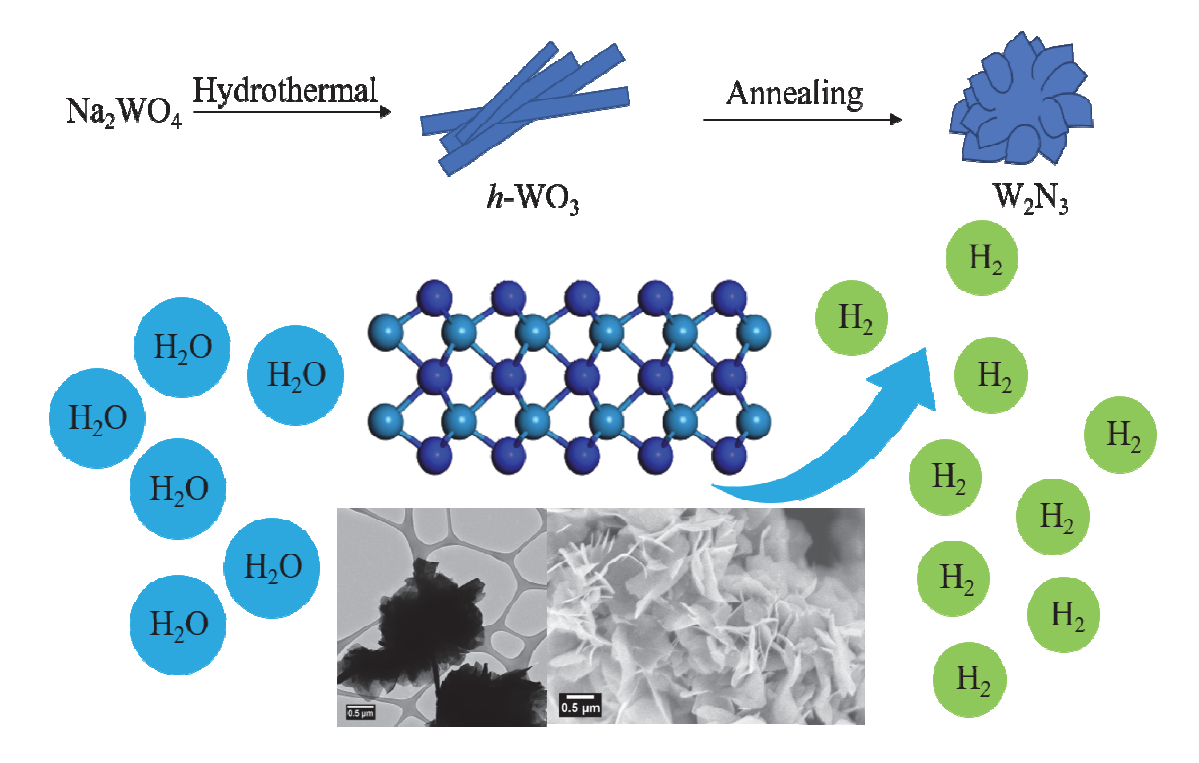


Figure 6. Measured (A) Faraday efficiencies, (B) current densities, and (C) CO/H_2 ratios of asprepared Au/W_2N_3 samples incorporating different Au sizes

TOC Figure



Flower-like motifs of nitrogen-rich tungsten nitride have been synthesized and applied as hydrogen evolution reaction catalysts in both acidic and alkaline environments. Upon deposition of metal nanoparticles onto the underlying tungsten nitride platforms, the resulting composites have been used as catalysts for both the methanol oxidation and CO₂ reduction reactions.